# Inversion of 2.5D electrical resistivity data using the discrete adjoint method

*Diego Domenzain*, Colorado School of Mines; John Bradford, Colorado School of Mines; Jodi Mead, Boise State University*

## SUMMARY

Joint inversion of different geophysical data can impose different grid discretization constraints on the sought model parameters. We present a 2.5D inversion algorithm of electrical resistivity (ER) data that requires low memory storage and can handle fine discretization domains imposed by other geophysical (e.g, ground penetrating radar or seismic) data. This enables the ER data sensitivities to be directly joined with other geophysical data without the need of interpolating or coarsening the discretization. We employ the adjoint method directly in the discretized Maxwell's steady state equation and make no finite difference approximation on the Jacobian of the data. Our algorithm is tested on synthetic and field data acquired in a controlled alluvial aquifer.

## INTRODUCTION

Electrical resistivity (ER) inversions that join other geophysical data are usefull tools for quantitatively characterizing subsurface properties. For example, Gallardo and Meju (2003) join ER with travel-time seismic data, and Doetsch et al. (2010) join ER with travel-time ground penetrating radar (GPR) data. Both of the mentioned methods linearize their respective wave propagation method. In doing so, the domain discretization is relaxed. Emerging inversion methods that use the full waveform of the data (for example, Domenzain et al. (2018) join ER with GPR data) demand finer discretization constraints (Courant et al., 1967).

Using second order inversion methods is common practice in most ER inversion schemes (Loke and Barker, 1996; Oldenburg and Li, 1999; Günther et al., 2006; Pidlisecky et al., 2007; Marescot et al., 2008). In Figure 1 we see in gray the amount in double precision memory needed to store the Hessian of the objective function for a range of domain sizes,

$$\text{2D Hessian memory} = (\#\text{ of pixels})^2. \tag{1}$$

In Ernst et al. (2007) the authors perform a 2D full-waveform inversion (FWI) of GPR borehole data on an aluvial aquifer, a setting with usual electrical parameters found in the subsurface. The number of pixels in their domain is roughly $10^5$. Commonly used ER inversion methods would require approximately $10^2$Gb of memory to store the Hessian.

In Loke and Barker (1996) and Pidlisecky et al. (2007) the authors approximate the Jacobian of the data with a finite difference scheme. In contrast, adjoint methods give direct access to the sensitivity of the data in the entire computational domain. The adjoint method for computing ER sensitivities can be applied by either considering the continuous objective function (Günther et al., 2006; Marescot et al., 2008), or the discrete objective function (Pratt et al., 1998; Ha et al., 2006). In Ha et al. (2006) the authors use the discrete adjoint method similar to Pratt et al. (1998) (in the context of acoustic FWI in the frequency domain) for computing a gradient descent direction in a 2D ER inversion. In their work it is shown that their 2D inversion method costs roughly the same number of flops as Gauss-Newton ER inversion techniques. However, their method does not account for 3D variability of the subsurface.

For our inversion method, we adapt the acoustic FWI of Pratt et al. (1998) to a 2D ER inversion. We use a gradient descent algorithm which relieves the need to store the Jacobian of the data, or approximate the Hessian of the objective function. Using the approximation of Pidlisecky and Knight (2008), we account for a 2.5D subsurface with our 2D forward model. In Pidlisecky and Knight (2008) the authors use a linear combination of 2D electric potentials to approximate the 2.5D solution. In their code it is noted that approximately only four 2D electric potentials suffice.

At most, the amount of memory for computing the ER sensitivities with our method is given by the memory needed to store four 2D electric potentials (4 copies of the domain), a 2D adjoint field (1 copy of the domain), and a 2D forward model matrix. With a rectangular grid discretization, each forward model matrix costs roughly five copies of the domain. In total we have $4 + 1 + 5 = 10$ copies of the domain,

$$\text{Our 2.5D method's memory} = \#\text{ of pixels} \cdot 10. \tag{2}$$

Given the low memory storage, our algorithm can be used for joint inversion with data whose forward models impose finer grid constraints without the need to interpolate the model parameters.

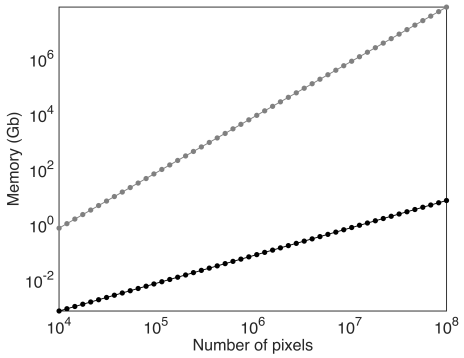


Figure 1: Memory needed to compute ER sensitivities as a function of domain size. In gray, using the Hessian of the objective function. In black, using our 2.5D approximation.

We assess the sensitivity of the recovered conductivity at depth using a measure of electric current density in our domain throughout all iterations. Our method relies on the physical

principle that the sensitivity of surface acquired ER data is given by electric current lines that return to the surface.

We show the usefulness of our work with a synthetic example and field data acquired at an alluvial acquifer near Boise, Idaho USA. For the ER field data, we compare our results with previous borehole studies at the same site (Oldenborger et al., 2007; Mwenifumbo et al., 2009) and find similar results for petrophysical parameters and conductivity values.

## METHODS

### ER 2.5D forward model

Assuming no variation along the $y$-axis, the physics of the ER experiment are given by (Dey and Morrison, 1979; Pidlisecky and Knight, 2008),

$$-\nabla\cdot\ \sigma(x,z)\nabla\,\varphi(x,y,z) = s(x,z), \tag{3}$$

where $\sigma$ is the electric conductivity, $\varphi$ is the electric potential, and $s$ is the electric current source. Equation 3 is solved by using the Fourier-cosine transform in the $k_y$-domain (Dey and Morrison, 1979; Pidlisecky and Knight, 2008),

$$-\nabla\cdot\ \sigma\nabla\,\tilde{\varphi}(x,k_y,z) + k_y^2\,\sigma\,\tilde{\varphi}(x,k_y,z) = \frac{1}{2}s(x,z), \tag{4}$$

and then integrating along the $k_y$ domain to get the solution $\phi$ in the $xz$-plane,

$$\varphi(x,y=0,z) = \frac{2}{\pi}\int_0^\infty \tilde{\varphi}\,\mathrm{d}k_y. \tag{5}$$

As detailed in Pidlisecky and Knight (2008) the discretized form of equation 4 demands computing weights $\boldsymbol{k}$ and $\boldsymbol{\omega}$. Both $\boldsymbol{k}$ and $\boldsymbol{\omega}$ are arrays of real numbers and of equal length.

Let $\boldsymbol{\sigma} > 0$ be the vector whose entries are the values for conductivity in our discretized domain. For each weight $k_i$ in $\boldsymbol{k}$ we discretize the differential operator of equation 4 as (Dey and Morrison, 1979),

$$\mathbf{L}_i = \mathbf{L}^i + k_i^2\,\boldsymbol{\sigma}. \tag{6}$$

The matrix $\mathbf{L}^i$ is the two-dimensional finite volume approximation of $-\nabla\cdot\ \sigma\nabla$. We impose Robin boundary conditions in the subsurface and Neumann boundary conditions on the air-ground surface. The Robin boundary conditions depend on $k_i$. The second term of equation 6 denotes a diagonal matrix with entries $k_i^2\,\boldsymbol{\sigma}$. For each weight $k_i$ the two-dimensional forwad model is,

$$\begin{aligned}\mathbf{L}_i\tilde{\boldsymbol{\varphi}}_i &= \frac{\mathbf{s}}{2},\\ \tilde{\mathbf{d}}_i &= \mathbf{M}\tilde{\boldsymbol{\varphi}}_i,\end{aligned} \tag{7}$$

where $\mathbf{M}$ is the measuring operator that transforms electric potential into voltage readings. The matrix $\mathbf{L}_i$ is square of size $n^2$ where $n$ is the total number of pixels in our domain. It is also sparse, where each row has a non-zero entry for each neighboring pixel and for itself. In the case of our rectangular grid, this matrix is sparse with 5 bands. Finally, equation 5 is discretized by,

$$\boldsymbol{\varphi} = \frac{2}{\pi}\sum_i \tilde{\boldsymbol{\varphi}}_i\,\omega_i. \tag{8}$$

Pidlisecky and Knight (2008) note that only four values of $k_i$ suffice for a good approximation of $\boldsymbol{\varphi}$.

### Inversion of 2.5D ER data

For a single source location our objective function is,

$$\Theta(\boldsymbol{\sigma};\,\mathbf{d}^o) = ||\mathbf{d}-\mathbf{d}^o||_2^2, \tag{9}$$

where $\mathbf{e} = \mathbf{d}-\mathbf{d}^o$ is the residual of the data. We compute the gradient $\mathbf{g}$ of $\Theta$ with respect to $\boldsymbol{\sigma}$ by,

$$\mathbf{g} = \mathbf{J}^\top\mathbf{e}, \tag{10}$$

where $\mathbf{J} = \nabla_\sigma\mathbf{d}$. The gradient operator $\nabla_\sigma$ is a row vector with the $i$'th entry being the partial derivative $\partial_{\sigma_i}$. In order to find an expression for $\mathbf{J}$ we first write $\mathbf{d}$ in terms of $\tilde{\mathbf{d}}_i$,

$$\mathbf{d} = \mathbf{M}\boldsymbol{\varphi} = \mathbf{M}\frac{2}{\pi}\sum_i \omega_i\tilde{\boldsymbol{\varphi}}_i, = \frac{2}{\pi}\sum_i \omega_i\mathbf{M}\tilde{\boldsymbol{\varphi}}_i = \frac{2}{\pi}\sum_i \omega_i\tilde{\mathbf{d}}_i. \tag{11}$$

We can now apply $\nabla_\sigma$ to equation 11,

$$\nabla_\sigma\mathbf{d} = \frac{2}{\pi}\sum_i \omega_i\mathbf{J}_i, \tag{12}$$

where $\mathbf{J}_i = \nabla_\sigma\tilde{\mathbf{d}}_i$. By substituting equation 12 in equation 10 we have,

$$\begin{aligned}\mathbf{g} &= \frac{2}{\pi}\left(\sum_i \omega_i\mathbf{J}_i\right)^\top\mathbf{e}\\ &= \frac{2}{\pi}\sum_i \omega_i\mathbf{J}_i^\top\mathbf{e}.\end{aligned} \tag{13}$$

Let $\tilde{\mathbf{g}}_i = \mathbf{J}_i^\top\mathbf{e}$. Equation 13 gives $\mathbf{g}$ (the 2.5D gradient) as a linear combination of 2D gradients $\tilde{\mathbf{g}}_i$. Using the adjoint method (Domenzain et al., 2017) we compute $\tilde{\mathbf{g}}_i$ by,

$$\begin{aligned}\mathbf{L}_i^\top\tilde{\mathbf{v}}_i &= \mathbf{M}^\top\mathbf{e},\\ \tilde{\mathbf{g}}_i &= \mathbf{S}_i\tilde{\mathbf{v}}_i,\end{aligned} \tag{14}$$

where

$$\mathbf{S}_i = -\left((\nabla_\sigma\mathbf{L}^i)\tilde{\boldsymbol{\varphi}}_i\right)^\top - k_i^2\,\mathrm{diag}(\tilde{\boldsymbol{\varphi}}_i)^\top, \tag{15}$$

The matrix $\mathbf{S}_i$ is sparse and has as many non-zero bands as $\mathbf{L}_i$ (five bands with a grid discretization). Finally, we compute the gradient $\mathbf{g}$ of equation 9 by,

$$\mathbf{g} = \frac{2}{\pi}\sum_i \omega_i\tilde{\mathbf{g}}_i. \tag{16}$$

The most memory expensive step to compute $\mathbf{g}$ is during equation 14. During this step four 2D electric potentials $\tilde{\boldsymbol{\varphi}}_i$ are stored, the adjoint field $\tilde{\mathbf{v}}_i$ is computed, and $\mathbf{S}_i$ is built (a five banded matrix). In total, ten copies of the domain.

### Regularization

We regularize the gradient $\mathbf{g}$ of equation 9 by adding the normalized residual of a reference conductivity $\boldsymbol{\sigma}_o$,

$$\mathbf{g} \leftarrow \mathbf{g} + \beta\frac{\boldsymbol{\sigma}-\boldsymbol{\sigma}_o}{\max(\mathrm{abs}(\boldsymbol{\sigma}-\boldsymbol{\sigma}_o))}, \tag{17}$$

where $\beta$ is a fixed number smaller than one.

Large values near the receiver locations arise when computing the gradient with the adjoint method (Taillandier et al., 2009;

Kurzmann et al., 2013). We smooth these artifacts using a space-frequency low-pass gaussian filter of width $\lambda$ (Taillandier et al., 2009; Domenzain et al., 2018),

$$\lambda = \frac{1}{\Delta r \cdot a}, \tag{18}$$

where $\Delta r$ is the electrode spacing in meters and $a$ is close to one, loosely $0.5 \leq a \leq 1.5$. After smoothing the gradient and normalizing by its largest amplitude we find the step size as proposed by Pica et al. (1990).

The final update $\Delta\boldsymbol{\sigma}$ is the average of all update directions over all source locations. When the sensitivity of our data is weak, $\Delta\boldsymbol{\sigma}$ might struggle to find a true descent direction. We address this issue using *momentum* (Rumelhart et al., 1986) which only costs the storage of the previous iteration update, $\Delta\boldsymbol{\sigma}_\bullet$. The final update for the conductivity is given by,

$$\begin{aligned} \Delta\boldsymbol{\sigma} &\leftarrow \Delta\boldsymbol{\sigma} + \beta_\bullet \Delta\boldsymbol{\sigma}_\bullet, \\ \boldsymbol{\sigma} &\leftarrow \boldsymbol{\sigma} \odot \exp(\boldsymbol{\sigma} \odot \Delta\boldsymbol{\sigma}), \end{aligned} \tag{19}$$

where $\beta_\bullet$ is a fixed number smaller than one. The update of the conductivity is taken in logarithmic space to ensure the positivity constraint (Meles et al., 2010).

### Solution appraisal

The sensitivity at depth of the ER survey is given by the electric current density of all shot-receiver pairs in the survey. Throughout the inversion, the illumination of the modeled subsurface changes as a function of the observed data and the initial conductivity model.

We quantify the total electric current density in our inversion by summing the absolute value of all 2.5D electric potentials $\boldsymbol{\varphi}$ over all iterations,

$$\Psi = \sum_i \sum_j |\boldsymbol{\varphi}_{ij}|, \tag{20}$$

where $j$ runs over source locations and $i$ over iterations. We choose the cut-off for our solution as the level curve beyond which the electric current lines on $\Psi$ no longer return to the surface.

## EXAMPLES

### Synthetic data

Figure 2**a** shows the synthetic scenario on which we test our algorithm. The model consists of a 20m by 4m subsurface domain with a 10mS/m cylindrical anomaly embedded in a 5mS/m background. We use 17 electrodes spaced 1m appart with all possible dipole-dipole, Wenner and Schlumberger arrays. The full discretized domain is of size $81 \times 401$ with a square pixel size of 0.05m.

The initial model is a homogeneous conductivity equal to the background of our model. For this example we set $\beta = 0$. We choose a smoothing factor of $a = 1.1$ (see equation 18) and a value of $\beta_\bullet = 0.02$.

The recovered conductivity in the entire computational domain is shown in Figure 2**b**. Figure 2**c** shows the recovered conductivity with a current density cut-off of 0.025% of the maximum value of $\Psi$ (see equation 20). We note that our solution appraisal technique removes parts of low sensitivity (bottom of the domain).

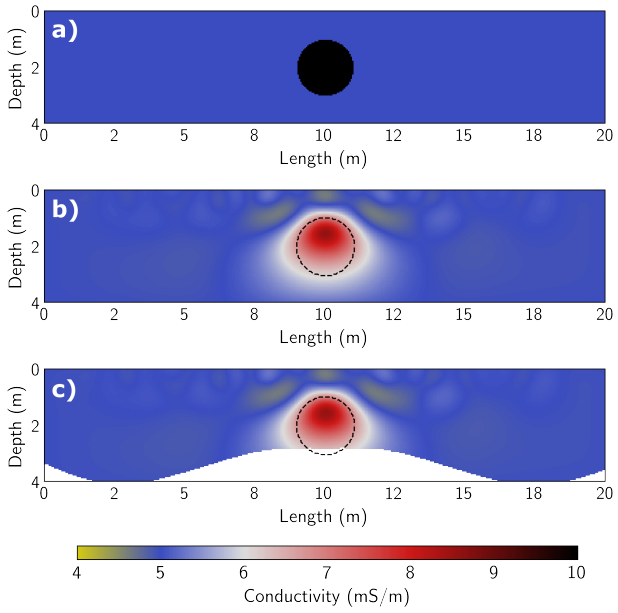


Figure 2: True **a**, recovered **b** and appraised **c** conductivity for the synthetic example. The dashed black line represents the contour of the cylinder.

### Field data

The data were acquired at the Boise Hydrological Research Site (BHRS) in May 2019. The site is an alluvial aquifer next to the Boise river (Barrash et al., 1999). A nearby dam controls the flow in the river throughout the year. We aimed our experiment to take place when the water table was at its highest point without the site being flooded. This choice was made to increase the electric current of our survey past the water table boundary and improve our depth sensitivity. We used an *IRIS Syscal Pro* resistivity system with a total of 36 electrodes spaced 1m apart in a one dimensional line perpendicular to the river. Our survey consisted of all possible dipole-dipole and Wenner arrays.

The position of the survey line was intended to enhance the variability of conductivity in the $xz$-plane whlie keeping the $y$ coordinate variability of the conductivity constant. This choice is based on previous knowledge of site stratigraphy (e.g. Bradford et al. (2009)).

Our initial model is a homogeneous subsurface with conductivity equal to 2mS/m. We regularize the inversion using a homogeneous reference conductivity equal to our initial model, and weighting factors of $\beta = 0.001$ and $\beta_\bullet = 0.5$. The full discretized domain is of size $301 \times 901$ with a square pixel size of 0.05m. Figure 3 gives the recovered conductivity corrected for topography and with a current density cut-off equal to 0.002% of the maximum value of $\Psi$ (see equation 20). Figure 4 shows the observed vs recovered data.



10.1190/segam2020-3417486.1

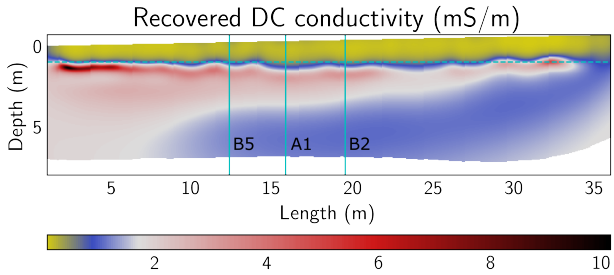


Figure 3: Recovered conductivity from the BHRS. The river is located towards the beginning of the survey line. The dashed cyan line represents the water table depth as measured on site (1m deep). The solid cyan lines represent the borehole positions. Note the higher conductivity, sand filled paleo channel that deepens toward the river.

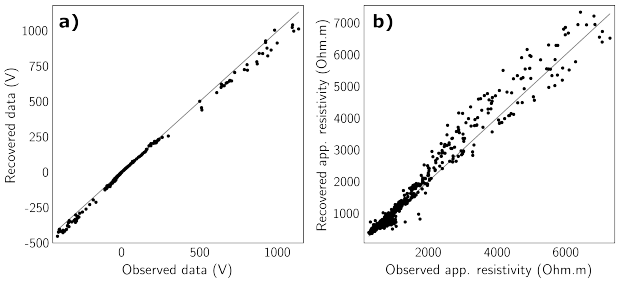


Figure 4: Observed vs recovered ER data acquired at the BHRS.

The water table depth was 1m and measured the same day the survey was done. Figure 3 shows that our recovered conductivity accurately images the water table boundary. We further note the higher conductivity, sand filled paleo channel that deepens toward the river is accurately represented.

We compare our inversion results following Oldenborger et al. (2007) who perform a time lapse borehole ER monitoring of the same site in Summer of 2004. Their analysis uses Archie's law (Archie et al., 1942) to compare the formation factor derived by ER recovered conductivity ($F_{ER}$) and the formation factor derived by neutron porosity logs ($F_{\varphi}$) acquired by Barrash and Clemo (2002).

| | B5 | A1 | B2 |
|---|---|---|---|
| $m$ | $1.7 \pm 0.3$ | $1.8 \pm 0.3$ | $1.6 \pm 0.1$ |
| $F_{ER}$ | $12.5 \pm 3$ | $13.3 \pm 3$ | $13.9 \pm 3$ |
| $F_{\phi}$ | $12.5 \pm 3$ | $13.3 \pm 3$ | $13.9 \pm 3$ |

Table 1: Formation and cementation factor appraisal for each borehole using recovered conductivity and neutron porosities. Our results correlate well to a previous borehole ER survey at the same site up to a standard deviation of at most ±1.

Oldenborger et al. (2007) give average values of $F_{ER} = 13 \pm 4$, $F_{\phi} = 13 \pm 4$ and cementation factor $m = 1.7$. In Table 1 we find similar values (within ±1 standard deviation) for $F_{ER}$, $F_{\phi}$ and $m$ with our recovered conductivity.

Figure 5 shows our recovered conductivity next to the capacitive conductivity as measured by Mwenifumbo et al. (2009). Their experiment was performed in the month of November, when the river water flow had significantly decreased to a 2m deep water table. Even though our experiments were performed with different ground water conditions, our recovered conductivity is within the same order of magnitude and follows close resemblance inside our appraised solution.

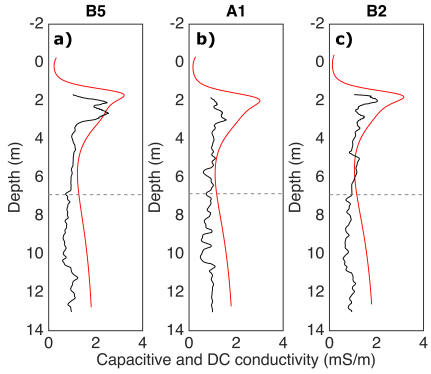


Figure 5: Recovered ER (with our method - in red) and capacitive conductivities (black) at borehole locations in the BHRS. The dashed gray line shows the cut-off for our appraised solution.

## CONCLUSIONS

We have developed an adjoint based method for inverting 2.5D electrical resistivity (ER) data. Our algorithm makes no assumption of the subsurface conductivity geometry. We directly obtain the sensitivity of the data in the entire domain and do not need to approximate the Jacobian of the data using finite differences. Moreover, we do not need to store large dense matricies (like the Jacobian of the data and the Hessian of the objective function). This enables us to very finely discretize the subsurface with feasible memory requirements. As a result, our algorithm can be used for joint inversion with data whose forward models impose finer grid constraints without the need to interpolate the model parameters.

In order to assess the quality of the recovered parameters, we use a measure of the electric current density present in our domain throughout iterations. This method for quality assessment takes into account the physics of the ER survey, the data and the model parameters throughout iterations.

We tested our algorithm on a synthetic example and on field data aquired at an alluvial aquifer near Boise, Idaho USA. We find good correlation of our field data results with neutron porosity and capacitive conductivity borehole measurements taken on the site in previous surveys.

## REFERENCES


Archie, G. E., 1942, The electrical resistivity log as an aid in determining some reservoir characteristics: Transactions of the AIME, **146**, 54–62, doi: https://doi.org/10.2118/942054-G.

Barrash, W., and T. Clemo, 2002, Hierarchical geostatistics and multifacies systems: Boise hydrogeophysical research site, boise, idaho: Water Resources Research, **38**, 14–14-18, doi: https://doi.org/10.1029/2002WR001436.

Barrash, W., T. Clemo, and M. D. Knoll, 1999, Boise hydrogeophysical research site (BHRS): objectives, design, initial geostatistical results: Symposium on the Application of Geophysics to Engineering and Environmental Problems, SEG, 389–398.

Bradford, J. H., W. P. Clement, and W. Barrash, 2009, Estimating porosity with ground-penetrating radar reflection tomography: A controlled 3-D experiment at the boise hydrogeophysical research site: Water Resources Research, **45**.

Courant, R., K. Friedrichs, and H. Lewy, 1967, On the partial difference equations of mathematical physics: IBM journal of Research and Development, **11**, 215–234, doi: https://doi.org/10.1147/rd.112.0215.

Dey, A., and H. Morrison, 1979, Resistivity modelling for arbitrarily shaped two-dimensional structures: Geophysical Prospecting, **27**, 106–136, doi: https://doi.org/10.1111/j.1365-2478.1979.tb00961.x.

Doetsch, J., N. Linde, and A. Binley, 2010, Structural joint inversion of time-lapse crosshole ert and gpr traveltime data: Geophysical Research Letters, **37**, doi: https://doi.org/10.1029/2010GL045482.

Domenzain, D., J. Bradford, and J. Mead, 2017, Imaging by joint inversion of electromagnetic waves and DC currents: Presented at the SIAM Mathematical and Computational issues in the Geosciences.

Domenzain, D., J. Bradford, and J. Mead, 2018, Joint inversion of gpr and er data: SEG Technical Program Expanded Abstracts, SEG, 4763–4767.

Ernst, J. R., A. G. Green, H. Maurer, and K. Holliger, 2007, Application of a new 2d time-domain full-waveform inversion scheme to crosshole radar data: Geophysics, **72**, J53–J64, doi: https://doi.org/10.1190/1.2761848.

Gallardo, L. A., and M. A. Meju, 2003, Characterization of heterogeneous near-surface materials by joint 2D inversion of dc resistivity and seismic data: Geophysical Research Letters, **30**, doi: https://doi.org/10.1029/2003GL017370.

Günther, T., C. Rücker, and K. Spitzer, 2006, Three-dimensional modelling and inversion of dc resistivity data incorporating topography—ii. inversion: Geophysical Journal International, **166**, 506–517, doi: https://doi.org/10.1111/j.1365-246X.2006.03011.x.

Ha, T., S. Pyun, and C. Shin, 2006, Efficient electric resistivity inversion using adjoint state of mixed finite-element method for poisson's equation: Journal of Computational Physics, **214**, 171–186, doi: https://doi.org/10.1016/j.jcp.2005.09.007.

Kurzmann, A., A. Przebindowska, D. Köhn, and T. Bohlen, 2013, Acoustic full waveform tomography in the presence of attenuation: a sensitivity analysis: Geophysical Journal International, **195**, 985–1000, doi: https://doi.org/10.1093/gji/ggt305.

Loke, M. H., and R. Barker, 1996, Rapid least-squares inversion of apparent resistivity pseudosections by a quasi- newton method 1: Geophysical prospecting, **44**, 131–152, doi: https://doi.org/10.1111/j.1365-2478.1996.tb00142.x.

Marescot, L., S. P. Lopes, S. Rigobert, and A. G. Green, 2008, Nonlinear inversion of geoelectric data acquired across 3d objects using a finite-element approach: Geophysics, **73**, no. 3. F121–F133, doi: https://doi.org/10.1190/1.2903836.

Meles, G. A., J. Van der Kruk, S. A. Greenhalgh, J. R. Ernst, H. Maurer, and A. G. Green, 2010, A new vector waveform inversion algorithm for simultaneous updating of conductivity and permittivity parameters from combination crosshole/borehole-to-surface gpr data: IEEE Transactions on geoscience and remote sensing, **48**, 3391–3407, doi: https://doi.org/10.1109/TGRS.2010.2046670.

Mwenifumbo, C. J., W. Barrash, and M. D. Knoll, 2009, Capacitive conductivity logging and electrical stratigraphy in a high-resistivity aquifer, boise hydrogeophysical research site: Geophysics, **74**, E125–E133, doi: https://doi.org/10.1190/1.3106760.

Oldenborger, G. A., P. S. Routh, and M. D. Knoll, 2007, Model reliability for 3d electrical resistivity tomography: Application of the volume of investigation index to a time-lapse monitoring experiment: Geophysics, **72**, no. 4, F167–F175, doi: https://doi.org/10.1190/1.2732550.

Oldenburg, D. W., and Y. Li, 1999, Estimating depth of investigation in dc resistivity and ip surveys: Geophysics, **64**, 403–416, doi: https://doi.org/10.1190/1.1444545.

Pica, A., J. Diet, and A. Tarantola, 1990, Nonlinear inversion of seismic reflection data in a laterally invariant medium: Geophysics, **55**, 284–292, doi: https://doi.org/10.1190/1.1442836.

Pidlisecky, A., E. Haber, and R. Knight, 2007, Resinvm3d: A 3d resistivity inversion package: Geophysics, **72**, H1–H10, doi: https://doi.org/10.1190/1.2402499.

Pidlisecky, A., and R. Knight, 2008, Fw2_5d: A matlab 2.5-d electrical resistivity modeling code: Computers and Geosciences, **34**, 1645–1654, doi: https://doi.org/10.1016/j.cageo.2008.04.001.

Pratt, R. G., C. Shin, and G. Hick, 1998, Gauss–newton and full newton methods in frequency–space seismic waveform inversion: Geophysical Journal International, **133**, 341–362, doi: https://doi.org/10.1046/j.1365-246X.1998.00498.x.

Rumelhart, D. E., G. E. Hinton, and R. J. Williams, 1986, Learning representations by back-propagating errors: Nature, **323**, 533, doi: https://doi.org/10.1038/323533a0.

Taillandier, C., M. Noble, H. Chauris, and H. Calandra, 2009, First-arrival traveltime tomography based on the adjoint- state method: Geophysics, **74**, WCB1–WCB10, doi: https://doi.org/10.1190/1.3250266.